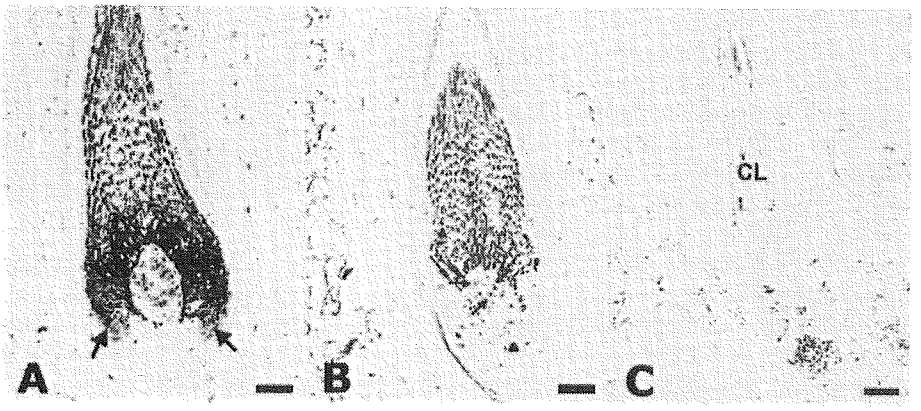

Fig. 3 In situ hybridization analysis of versican during the human hair cycle. Human scalp-skin sections were stained with the anti-sense RNA probe for the conserved domain of four versican isoforms. (A) In anagen hair follicles, the DP and bulb matrix (large arrows) showed positive signals for versican mRNA. (B) Very weak staining (small arrows) was observed in the upper portion of the DP in early-mid catagen hair follicles, which were identified by the constriction of bulb matrix compared to anagen hair follicles. (C) The positive signal was barely seen in telogen hair follicles, which were distinguished by the fully keratinized club (CL) above the condensed DP [scale bars, 50 μm].

3.2. Specific accumulation of versican protein in the DP during the anagen phase and in the bulge during the hair cycle

During the human hair cycle, versican immunofluorescence was intense in the DP of anagen hair follicles (Fig. 4A). This immunofluorescence observed in the DP was diminished in the catagen phase (Fig. 4B), consistent with the gene expression pattern of versican described above (see Fig. 3B). Interestingly, the DP of telogen hair follicles showed faint immunofluorescence (Fig. 4C) although mRNA was not detectable during this phase (see Fig. 2C). Strong versican immunofluorescence was also observed in the connective tissue sheath surrounding the bulge region in anagen (data not shown), catagen (Fig. 4B), and telogen (Fig. 4C), but not the lower bulb of anagen hair follicles (Fig. 4A).

We performed double-immunofluorescence labeling combined with anti-K15 antibody and anti-versican antibody to confirm versican deposition around the bulge region of hair follicles (Fig. 5). Versican immunofluorescence (green colors) was detected in the connective tissue sheath along with K15-positive (red colors) follicular epithelial cells below the sebaceous gland in anagen hair follicles (Fig. 5A). In K15-positive cells, intense K15 immunofluorescence was restricted to the outer side adjacent to the connective tissue sheath (Fig. 5B; higher magnification around K15-positive cells).

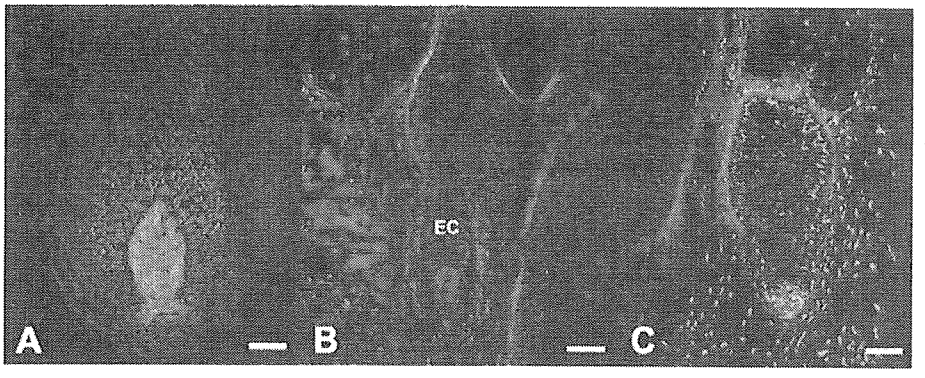

Fig. 4 Immunofluorescence staining of versican during the human hair cycle. Localization of versican proteins was analyzed by immunofluorescence staining in human hair follicles in anagen, catagen, and telogen phases. Red staining represented positive versican immunofluorescence, and blue staining indicated nuclei. (A) Only the DP was intensely stained in the lower portion of anagen hair follicles. (B) In late catagen hair follicles characterized by the epithelial column (EC), the DP was almost negative for versican immunofluorescence staining. (C) The DP was weakly positive for versican immunofluorescence staining in the telogen phase. The connective tissue sheath surrounding the bulge region showed intense immunofluorescence for versican in telogen hair follicles as well as anagen (see Fig. 5 and catagen follicles (B) [scale bars, 50 μm].

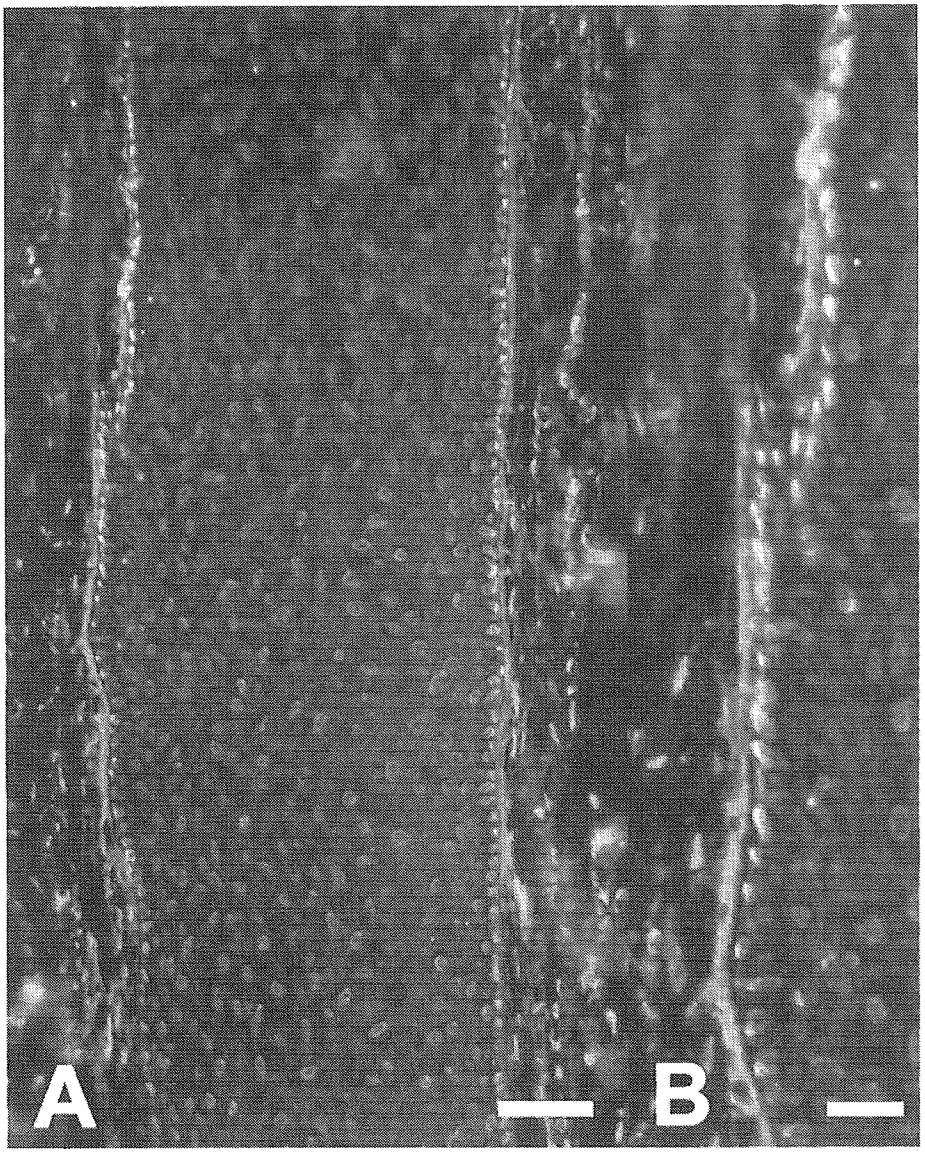

Fig. 5 Double immunofluorescence labeling of the bulge region with versican and K15 in anagen hair follicles. The sites of versican immunofluorescence were compared with the sites of K15 immunofluorescence around the bulge region in human anagen hair follicles. (A) Strong versican immunofluorescence (green) in the connective tissue sheath was localized outside of K15 (red)-positive cells. Blue staining indicated nuclei [scale bar, 50 μm]. (B) Higher magnification around K15-positive cells. Intense K15 immunofluorescence (red) was observed in the outermost portion of K15-positive ORS cells [scale bar, 20 μm].

3.3. Lower versican level in vellus-like hair follicles of male pattern baldness

To investigate whether versican expression is related to male pattern baldness, we examined both the gene and protein expression level of versican in vellus-like hair follicles observed in male pattern baldness. Versican gene expression is almost lost in the DP of vellus-like hair follicles in the anagen phase (Fig. 6A). Versican immunoreactivity was significantly lower in the DP of vellus-like hair follicles (Fig. 6B) compared to terminal hair follicles (Fig. 4A) although the dermal components surrounding the vellus-like hair follicles appeared positive for versican immnostaining. The apparent down-regulation of versican expression was confirmed by more than 15 vellus-like hair follicles in balding scalp-skin tissues derived from three individuals (at least five vellus per each individual).

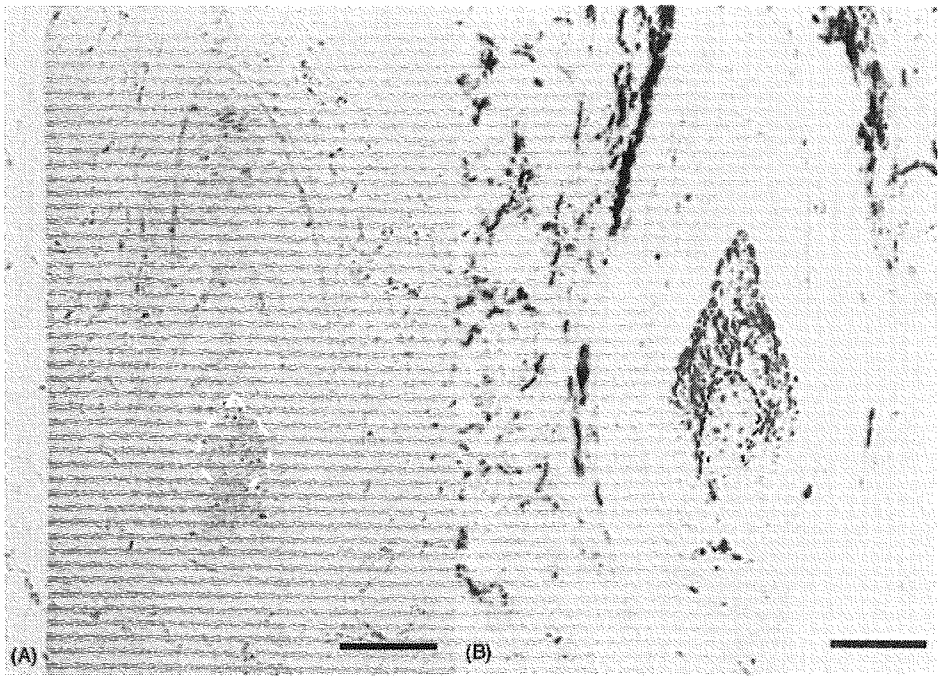

Fig. 6 Analysis of versican expression in vellus-like hair follicles affected by androgenic alopecia. (A) Versican transcripts (blue) were barely detected in the DP (white broken outline) of vellus-like hair follicles, which were distinguished from normal hair follicles by the miniature DP (B) Versican immunoreactivity (blue green) was detected in the fibrous dermal tissues surrounding vellus-like hair follicles but not almost lost in the DP (black broken outline). Red staining indicated nuclei [scale bars, 50 μm].

4. Discussion

In this study, we showed the anagen-specific expression of versican in the DP during human hair cycle, similar to mouse species. In addition, versican expression was diminished in the DP of vellus-like hair follicles affected by androgenic alopecia. These results show that versican is required for normal human hair growth.

At least four isoforms of the versican gene exist as variants by alternative splicing [12,13]. Interestingly, two isoforms (V2 and V3) are dominant in in vivo hair follicles in contrast to cultured DP cells, which harbor V0 and V1 isoforms as their major forms. The tissue-restricted expression pattern of versican variants was also observed in other human adult tissues [14]. The elevation and/or diminution of the definite variant forms have been shown during the developmental stage of the neural crest [15]. In addition, overexpression of the V3 variant, which has no binding domain of chondroitin sulfate, alters arterial smooth muscle cell adhesion, migration, and proliferation in vitro [14,16]. A distinct expression pattern between in vivo and in vitro may provide valuable information about the hair inductive ability of human DP cells. In mice, the same V3 variant was also dominantly expressed in DP cells, implicating the improvement of hair induction with this non-chondroitin sulfate proteoglycan. It should be examined using in vivo grafting assays whether the overexpression of a definite versican isoform in human cultured DP cells can restore their hair inductive ability.

The tissue-restricted distribution of versican variants was also confirmed at their protein level using several anti-versican antibodies, whose epitope had been already mapped [14]. As clone 2-B-1 used in this study is known to bind specifically to the C-terminal globular domain common to all four isoforms of human versican [10], the immunoreactivity described here showed the entire immunoreactivity for versican. In mouse and rat hair follicles, versican immunoreactivity is very intense and specific in the anagen phase of the mature hair cycle. In this study, human hair follicles also showed specific accumulation of versican proteins in the DP in the anagen phase. The apparent diminution of versican immunoreactivity was observed in catagen hair follicles identical to the mouse species [6]. Since the predominant gene expression of versican continued until just before catagen entry (Fig. 3B), continuous versican gene expression throughout the anagen phase seems necessary for the maintenance of normal hair growth. In the dermis, no versican tran-

script was detected despite abundant versican IR. These observations are consistent with the expression pattern of the transgene in the dorsal skin of versican transgenic mice [6], and DP-derived versican may serve as source of interfollicular immunoreactivity of versican.

Recent developments have shown that the stem cells of the follicular epithelium exist in the bulge region below the sebaceous gland. K15 is preferentially expressed in bulge cells, and its promoter could target hair follicle bulge cells [17,18]. Surprisingly, versican protein was deposited outside of K15-positive epithelial cells in the bulge area during human hair cycle. Since versican protein was slightly deposited in the DP of telogen hair follicles without its gene expression, versican protein derived from the bulge area may be incorporated into the DP before the next anagen entry. Versican deposition around the bulge also correlated with a previous report showing the relationship between versican and innervation [19], which demonstrated that versican was associated with nerve fibres during the development of rat vibrissa hair follicles.

Although proteoglycans are involved in hair morphogenesis and hair cycling [4,6], the correlation between hair follicle-related disorders and proteoglycans, including versican, remains unclear. For example, the abnormal accumulation of glycosaminoglycans leads to thick hair with a faster growth rate during childhood in Mucopolysaccharidoses (Hurler's syndrome) [3]. Here, we first showed the low expression of versican in vellus-like hair follicles affected by androgenic alopecia (Fig. 6). This lower expression of versican in androgenic alopecia is considerably regulated at its transcriptional level since mRNA is not detectable in the dermal papilla of vellus-like hair follicles in the anagen stage (Fig. 6A). Although the minimal promoter region of the human versican gene was reported by Naso et al. [20], no functional binding site of the androgen receptor has been identified in this promoter sequence. Some potent androgen responsive elements may be located in the regulatory sequence of the versican gene.

Acknowledgment

The authors would like to thank Dr Tetsuo Ezaki for his cooperation in obtaining materials.

References

[1] Jones FS, Jones PL. The tenascin family of ECM glycoproteins: structure, function, and regulation during embryonic development and tissue remodelling. Dev Dyn 2000;218: 235–59.

[2] Perrimon N, Bernfield M. Specificities of heparan sulphate proteoglycans in developmental processes. Nature 2000;404:725–8.

[3] Muenzer J. Mucopolysaccharidoses. Adv Pediatr 1986;33: 269–302.

[4] Westgate GE, Messenger AG, Watson LP, Gibson WT. Distribution of proteoglycans during the hair growth cycle in human skin. J Invest Dermatol 1991;96:191–5.

[5] Shinomura T, Nishida Y, Ito K, Kimata K. cDNA cloning of PG-M, a large chondroitin sulfate proteoglycan expressed during chondrogenesis in chick limb buds. Alternative spliced multiforms of PG-M and their relationships to versican. J Biol Chem 1993;268:14461–9.

[6] Kishimoto J, Ehama R, Wu L, Jiang S, Jiang N, Burgeson RE. Selective activation of the versican promoter by epithelial–mesenchymal interactions during hair follicle development. Proc Natl Acad Sci USA 1999;96: 7336–41.

[7] du Cros DL, LeBaron RG, Couchman JR. Association of versican with dermal matrices and its potential role in hair follicle development and cycling. J Invest Dermatol 1995;105:426–31.

[8] Harris SJ, Jahoda CA. A correlation between versican and neurofilament expression patterns during the development and adult cycling of rat vibrissa follicles. Mech Dev 2001;101:227–31.

[9] Sorrell JM, Carrino DA, Baber MA, Caplan AI. Versican in human fetal skin development. Anat Embryol 1999;199:45–56.

[10] Isogai Z, Shinomura T, Yamakawa N, Takeuchi J, Tsuji T, Heinegard D, et al. 2-B-1 antigen characteristically expressed on extracellular matrices of human malignant tumors is a large chondroitin sulfate proteoglycan, PG-M/versican. Cancer Res 1996;56:3902–8.

[11] Nitta H, Kishimoto J, Grogan TM. Application of automated mRNA in situ hybridization for formalin-fixed, paraffin-embedded mouse skin sections: effects of heat and enzyme pretreatment on mRNA signal detection. Appl Immunohistochem Mol Morphol 2003;11:183–7.

[12] Dours-Zimmermann MT, Zimmermann DR. A novel glycosaminoglycan attachment domain identified in two alternative splice variants of human versican. J Biol Chem 1994;269:32992–8.

[13] Zako M, Shinomura T, Ujita M, Ito K, Kimata K. Expression of PG-M(V3), an alternatively spliced form of PG-M without a chondroitin sulfate attachment in region in mouse and human tissues. J Biol Chem 1995;270:3914–8.

[14] Cattaruzza S, Schiappacassi M, Ljungberg-Rose A, Spessotto P, Perissinotto D, Morgelin M, et al. Distribution of PG-M/versican variants in human tissues and de novo expression of isoform V3 upon endothelial cell activation, migration, and neoangiogenesis in vitro. J Biol Chem 2002;277: 47626–35.

[15] Perissinotto D, Iacopetti P, Bellina I, Doliana R, Colombatti A, Pettway Z, et al. Avian neural crest cell migration is diversely regulated by the two major hyaluronan-binding proteoglycans PG-M/versican and aggrecan. Development 2000;127:2823–42.

[16] Lemire JM, Merrilees MJ, Braun KR, Wight TN. Overexpression of the V3 variant of versican alters arterial smooth muscle cell adhesion, migration, and proliferation in vitro. J Cell Physiol 2002;190:38–45.

[17] Liu Y, Lyle S, Yang Z, Cotsarelis GS. Keratin 15 promoter targets putative epithelial stem cells in the hair follicle bulge. J Invest Dermatol 2003;121:963–8.

[18] Lyle S, Christofidou-Solomidou M, Liu Y, Elder DE, Albelda S, Cotsarelis G. Human hair follicle bulge cells are biochemically distinct and possess an epithelial stem cell phenotype. J Invest Dermatol Symp Proc 1999;4:296–301.
[19] Harris SJ, Jahoda CA. A correlation between versican and neurofilament expression patterns during the development and adult cycling of rat vibrissa follicles. Mech Dev 2001;101:227–31.
[20] Naso MF, Zimmermann DR, Iozzo RV. Characterization of the complete genomic structure of the human versican gene and functional analysis of its promoter. J Biol Chem 1994;269:32999–3008.

STEM CELLS®
Original Article

Establishment of Novel Embryonic Stem Cell Lines Derived from the Common Marmoset (*Callithrix jacchus*)

ERIKA SASAKI,[a] KISABURO HANAZAWA,[b] RYO KURITA,[c] AKIRA AKATSUKA,[d] TAKAHITO YOSHIZAKI,[e] HAJIME ISHII,[a] YOSHIKUNI TANIOKA,[a] YASUYUKI OHNISHI,[f] HIROSHI SUEMIZU,[f] AYAKO SUGAWARA,[g] NORIKAZU TAMAOKI,[f] KIYOKO IZAWA,[h] YUKOH NAKAZAKI,[c] HIROMI HAMADA,[i] HIROFUMI SUEMORI,[j] SHIGETAKA ASANO,[h] NORIO NAKATSUJI,[k] HIDEYUKI OKANO,[e] KENZABURO TANI[c]

[a]Division of Laboratory Animal Science, Central Institute for Experimental Animals, Kawasaki, Kanagawa, Japan; [b]Department of Urology, Urayasu Hospital, Juntendo University, Urayasu, Chiba, Japan; [c]Department of Molecular Genetics, Division of Molecular and Clinical Genetics, Medical Institute of Bioregulation, Kyushu University, Hakata, Fukuoka, Japan; [d]Tokai University School of Medicine, Isehara, Kanagawa, Japan; [e]Department of Physiology, Keio University School of Medicine, Shinjuku-ku, Tokyo, Japan; [f]Research Project Center, [g]Department of Genetics, Central Institute for Experimental Animals, Kawasaki, Kanagawa, Japan; [h]Division of Molecular Therapy, Institute of Medical Science, University of Tokyo, [i]Institute of Obstetrics & Gynecology in Clinical Medicine, University of Tsukuba, [j]Laboratory of Embryonic Stem Cell Research, Stem Cell Research Center, [k]Department of Development and Differentiation, Institute for Frontier Medical Sciences, Kyoto University, Kyoto, Japan

Key Words. Embryonic stem cells • Common marmoset • Embryoid body • Nonhuman primate • Teratoma formation

ABSTRACT

The successful establishment of human embryonic stem cell (hESC) lines has inaugurated a new era in regenerative medicine by facilitating the transplantation of differentiated ESCs to specific organs. However, problems with the safety and efficacy of hESC therapy in vivo remain to be resolved. Preclinical studies using animal model systems, including nonhuman primates, are essential to evaluate the safety and efficacy of hESC therapies. Previously, we demonstrated that common marmosets are suitable laboratory animal models for preclinical studies of hematopoietic stem cell therapies. As this animal model is also applicable to preclinical trials of ESC therapies, we have established novel common marmoset ESC (CMESC) lines. To obtain marmoset embryos, we developed a new embryo collection system, in which blastocysts can be obtained every 3 weeks from each marmoset pair. The inner cell mass was isolated by immunosurgery and plated on a mouse embryonic feeder layer. Some of the CMESC lines were cultured continuously for more than 1 year. These CMESC lines showed alkaline phosphatase activity and expressed stage-specific embryonic antigen (SSEA)-3, SSEA-4, TRA-1-60, and TRA-1-81. On the other hand, SSEA-1 was not detected. Furthermore, our novel CMESCs are pluripotent, as evidenced by in vivo teratoma formation in immunodeficient mice and in vitro differentiation experiments. Our established CMESC lines and the common marmoset provide an excellent experimental model system for understanding differentiation mechanisms, as well as the development of regenerative therapies using hESCs. STEM CELLS *2005;23:1304–1313*

Correspondence: Kenzaburo Tani, M.D., Ph.D., Department of Molecular Genetics, Division of Molecular and Clinical Genetics, Medical Institute of Bioregulation, Kyushu University, Hakata, Fukuoka 812-8582, Japan. Telephone: 81-92-642-6434; Fax: 81-92-642-6444; e-mail: taniken@bioreg.kyushu-u.ac.jp; for CMES cell distribution, contact Erika Sasaki at esasaki@cica.or.jp Received December 22, 2004; accepted for publication May 5, 2005; first published online in STEM CELLS *EXPRESS* August 18, 2005. ©AlphaMed Press 1066-5099/2005/$12.00/0 doi: 10.1634/stemcells.2004-0366

Introduction

Embryonic stem cells (ESCs) are derived from preimplantation embryos. Owing to their pluripotency, ESCs have been widely used for the production of transgenic and gene knockout mice to elucidate the molecular mechanisms of various genes. In 1998, the successful establishment of human ESC (hESC) lines enhanced the role of ESCs in science and medicine. The most promising application of ESCs in the clinical setting is in the repair of defective organ function by differentiated ESCs. However, before differentiated hESCs can be used in clinical applications, the short-term and long-term safety and efficacy of ESCs must be thoroughly examined. Due to ethical considerations, these studies cannot be performed in vivo in humans. Therefore, preclinical studies using the ESCs of nonhuman primates are essential.

The common marmoset (*Callithrix jacchus*) is a New World primate species with reproductive characteristics that are appropriate for ESC studies. More specifically, these animals are small (weighing approximately 350–400 g), they have a short gestation period (approximately 144 days), and reach sexual maturity at 12–18 months. Unlike macaques, marmosets routinely deliver twins or triplets for each pregnancy. In addition, it is possible to synchronize the marmoset ovarian cycle with prostaglandin analogs, collect age-matched embryos from multiple females, and transfer embryos to synchronized recipients with success rates in the range of 70%–80% [1–3]. Because these reproductive characteristics allow routine efficient transfer of multiple embryos, marmosets constitute an excellent primate species for the generation of transgenic and knockout animal models of human diseases.

In addition to these reproductive benefits, we have shown previously that marmosets are suitable laboratory animals for preclinical studies of stem cell therapies, owing to the similarities between the hematopoietic and immune systems of humans and marmosets [4, 5]. In 1996, Thomson et al. [6] established pluripotent common marmoset cell lines, which are considered powerful tools for understanding the regulatory mechanisms of ESC differentiation both in vitro and in vivo. However, the differentiation abilities of the pluripotent common marmoset cells in terms of in vitro teratoma formation assays and certain common properties of ESC lines, such as differentiation to the cell lineages of three germ layers, have not been defined fully. The establishment of totipotent common marmoset ESC (CMESC) lines would facilitate the construction, by gene targeting, of nonhuman primate models for human disease. To achieve our goal of establishing the common marmoset as a human disease model, we have established novel CMESC lines and characterized their differentiation capacities.

Materials and Methods

Animals

To obtain marmoset embryos, 15 pairs of common marmosets, older than 2 years of age, were selected from the marmoset breeding colony; this colony has been maintained in our laboratory at the Central Institute for Experimental Animals (CIEA) since 1975. Each pair was kept in a cage with dimensions of 39 × 60 × 70 cm. This study was approved by the animal ethics committees of CIEA and was performed in accordance with CIEA guidelines.

Embryo Collection

Fifteen female animals were divided into three groups. The ovulation cycles of each group of animals were synchronized with the prostaglandin (PG) F2α analogue cloprostenol (0.75 mg/head Estrumate; Schering-Plough Animal Health, Union, NJ, http://www.spah.com) which was administered more than 10 days after the luteal phase, as reported previously [7]. Plasma samples (0.1 ml) were collected from the femoral vein at 2, 9, 11, and 13 days after the injection of cloprostenol, and the day of ovulation was determined by the plasma progesterone concentration, using an enzyme immunoassay (EIA), as described below. The day of ovulation (day 0) was defined as the day before the serum progesterone level reached 10 ng/ml [8]. Embryos were collected 7–10 days after ovulation, after anesthesia by intramuscular injection of 0.05 mg per head of medetomidine hydrochloride (Domitor; Meiji Techno, Tokyo, http://www.meijitechno.co.jp) or 0.25–0.5 mg per head of flunitrazepam (Silece; Eisai Co., Ltd., Tokyo, http://www.eisai.co.jp/index-e.html) and 70 mg per head of ketamine hydrochloride (veterinary Ketalar 50; Sankyo Lifetech Co., Ltd., Tokyo, http://www.sankyo-lifetech.co.jp/english). The cervix and both oviducts were exteriorized by midline laparotomy and clamped, and the uterine lumen was flushed from the proximal end to the cervix with 2.5 ml of Dulbecco's modified Eagle's medium (DMEM; Invitrogen, Tokyo, http://www.invitrogen.com) that contained 10% fetal bovine serum (FBS; JRH, Tokyo, http://www.jrhbio.com). The flushed medium was collected using a 23-gauge needle that was placed in the uterine lumen through the uterine fundus. Cloprostenol was also administered 4 days after embryo collection. The plasma progesterone concentration was determined using the DPC Progesterone Kit (Diagnostic Products Corporation, Los Angeles, http://www.dpcweb.com) according to the recommendations of the manufacturer.

Isolation and Culture of ESC Lines

Inner cell masses (ICMs) were isolated by immunosurgery, as described previously [9]. Briefly, the zona pellucida of the marmoset blastocyst was removed by the addition of 0.5% pronase (Sigma, Tokyo, http://www.sigmaaldrich.com) in DMEM, and the blastocysts were washed three times with DMEM. To remove the trophectoderm, the blastocysts were incubated for 45 minutes at 37°C in 5% CO_2 with a 10-fold dilution of anti-marmoset fibroblast rabbit serum in DMEM. After three washes with DMEM, the blastocysts were incubated with a fivefold dilution of guinea pig complement (Invitrogen) in DMEM for 30 minutes at 37°C in 5% CO_2. After immunosurgery, the trophectoderm was removed by pipet-

ting, and the ICMs were isolated. The ICMs were plated on 3,500-rad γ-irradiated mouse embryonic fibroblast (MEF) feeder layer. After 10–14 days, the ICMs were dissociated in trypsin-EDTA and replated on a fresh MEF feeder layer. The ICMs and their expanded cells were cultured using CMESC medium that consisted of 80% Knockout DMEM supplemented with 20% Knockout Serum Replacement (KSR; Invitrogen), 1 mM L-glutamine, 0.1 mM MEM nonessential amino acids, 0.1 mM β-mercaptoethanol (2-ME; Sigma), 100 IU/ml penicillin, 100 μg/ml streptomycin sulfate, 250 ng/ml amphotericin B, and 10 ng/ml leukemia inhibitory factor. For cell splitting, undifferentiated CMESC colonies were detached from the feeder cells, using 0.25% trypsin that was supplemented with 1 mM $CaCl_2$ and 20% KSR. The removed colonies were mechanically dissociated into 10 to 50 cells and replated on new irradiated MEF feeder layer.

Immunohistochemical Staining

To examine the expression of cell surface markers on cultured marmoset ICMs, alkaline phosphatase was detected using the Alkaline Phosphatase Staining Kit (Sigma) according to the manufacturer's instructions. For immunostaining, ESCs were fixed with 4% paraformaldehyde in phosphate-buffered saline (PBS) for 10 minutes at room temperature and then incubated with 0.3% H_2O_2 for 10 minutes at room temperature. The primary antibodies against stage-specific embryonic antigen (SSEA)-1, SSEA-3, SSEA-4 (Developmental Studies Hybridoma Bank, Iowa City, IA, http://www.uiowa.edu/~dshbwww), TRA-1-60, and TRA-1-81 (Chemicon, Temecula, CA, http://www.chemicon.com) were diluted with Antibody Diluent (DAKO ChemMate; DakoCytomation, Glostrup, Denmark, http://www.dakocytomation.dk) and incubated for 1 hour at room temperature. The following primary antibodies (dilutions) were used: anti-SSEA-1 (1:50), anti-SSEA-3 (1:10), anti-SSEA-4 (1:50), anti-TRA-1-60, and anti-TRA-1-81 (10 μg/ml). After three washes with PBS, the biotinylated secondary antibody Simple Stain PO Multi system (Nichirei Corporation, Tokyo, http://www.nichirei.co.jp/english) was incubated with the cells for 30 minutes at room temperature. The samples were washed three times with PBS, and the localization of the bound monoclonal antibodies was detected using the DAB (3,3'-diaminobenzidine tetrahydrochloride) horseradish peroxidase complex.

For immunohistochemical analysis of tumors that formed after transplantation into immunodeficient mice, the collected tumors were fixed in neutral buffered formalin and embedded in paraffin. The paraffin blocks were sectioned and subjected to immunohistochemical staining. Primary antibodies against keratin wide specific screening (WSS), desmin, CD31, and glial fibrillary acidic protein (GFAP) (all purchased from DakoCytomation, Tokyo) were incubated with the paraffin sections at dilutions of 1:200, 1:200, 1:10, and 1:50, respectively. The localization of the bound monoclonal antibodies was detected using the Envision System (DakoCytomation).

For immunofluorescence staining of in vitro–differentiated neural cells, the slides and sections were preincubated with 10% normal goat serum plus 0.3% Triton X-100 in PBS, followed by overnight incubation in 10% normal goat serum plus 0.3% Triton X-100 in PBS that contained rabbit polyclonal anti-TH antibody (AB152; Chemicon). Alexa™ 488 goat anti-rabbit IgG antibody and Alexa™ 568 goat anti-mouse IgG antibody (Jackson ImmunoResearch Laboratories, Inc., West Grove, PA, http://www.jacksonimmuno.com) were added as secondary antibodies for 2 hours. Finally, the specimens were soaked in 2 μg/ml Hoechst 33528 in distilled water. All of the micrographs were analyzed on the Zeiss AxioCam imaging system (Carl Zeiss, Jena, Germany, http://www.zeiss.com).

Karyotypic Analysis

ESCs were prepared by passaging a confluent culture from a 25-cm^2 bottle. After a 3-hour incubation with fresh medium, a colcemid (Invitrogen) was added to a final concentration of 0.02 μg/ml for 20 minutes. The cells were then washed in PBS, dissociated using trypsin, and spun down. The pellet was resuspended carefully in 0.56% KCl at room temperature. After centrifugation, the hypotonic solution was removed, and the pellet was fixed with methanol/acetic acid, 3:1 (vol/vol) via gently pipetting. After centrifuging at 1,000 rpm, 5-minute fixation was performed twice before spreading the cells on slides. The slides were air-dried overnight, stained in freshly made 5% Giemsa for 10 minutes, and rinsed with distilled water. In the Giemsa (G)-banding analysis, the numbers of chromosomes as well as karyotypic analysis were performed using 30 and five metaphase spreads, respectively.

Telomerase Activity

Telomerase activity was determined using the TRAPEZE Telomerase Detection Kit (Chemicon, Tokyo) according to the manufacturer's instructions. Briefly, cell extracts were obtained from approximately 1×10^6 cells, and the protein concentrations were normalized using the Coomassie blue–stained protein assay reagent bovine serum albumin standards (Pierce, Inc., Rockford, IL, http://www.piercenet.com). Heat-inactivated controls were obtained by incubating the samples at 85° C for 10 minutes. Aliquots (1.5 μg) of the cell extracts were used for polymerase chain reaction (PCR), which was performed according to the manufacturer's instructions. The PCR products were electrophoresed on a 12.5% nondenaturing polyacrylamide gel, and telomerase activity was detected by SYBR green staining (Invitrogen).

PCR–Single Strand Conformation Polymorphism (PCR-SSCP)

SSCP analysis of the major histocompatibility complex-DRB genes was performed as described previously [10]. The following PCR primers were used: MA-DR-2r, 5'-CTCTCCGCGGCACTAGGAAC-3'; and MA-DR-4s, 5'-GCACGTTTCTTGGAGTATAGC-3'.

Reverse Transcription (RT)–PCR

Poly(A)$^+$ RNA was isolated using the QuickPrep Micro mRNA Purification Kit (GE Healthcare, Toyko, http://www4.amershambioscience.com) according to the manufacturer's instructions. First-strand cDNA was synthesized from 1 μg of poly(A)$^+$ RNA from the undifferentiated ESCs, or the embryoid bodies (EBs), using the ImProm-II cDNA Synthesis Kit (Promega, Tokyo, http://www.promega.com). As negative controls, 1 μg of the poly(A)$^+$ RNA was allowed to react with the cDNA synthesis reaction mixture in the absence of the ImProm-II RT. After cDNA synthesis, 1/20 of the cDNA synthesis reaction mixture was used as the template for the PCR. For RT-PCR analysis of fresh ICMs, ICMs were obtained from seven blastocysts and used for poly(A)$^+$ RNA isolation. Half of the isolated poly(A)$^+$ RNA was then used for first-strand cDNA synthesis, and the other half was used as a negative control, as described above.

Individual primers were designed for the target genes. The following (forward and reverse) primer pairs were used: *Nanog*, 5'-AAACAGAAGACCAGAACTGTG-3' and 5'-AGTTGTTTTTCTGCCACCTCT-3'; *Oct3/4*, 5'-CCTGGGGGTTCTATTTGGGA-3' and 5'-TTTGAATGCATGGGAGAGCC-3'; *FoxD3*, 5'-CGACGACGGGCTGGAGGAGAA-3' and 5'-ATGAGCGCGATGTACGAGTA-3'; *Sox-2*, 5'-AGAACCCCAAGATGCACAAC-3' and 5'-GGGCAGCGTGTACTTATCCT-3'; CD34, 5'-AGCCTGTCACCTGGAAATGC-3' and 5'-CGTGTTGTCTTGCTGAATGGC-3'; *Nestin*, 5'-GCCCTGACCACTCCAGTTTA-3' and 5'-GGAGTCCTGGATTTCCTTCC-3'; *α-fetoprotein*, 5'-GCTGGATTGTCTGCAGGATGGGGAA-3' and 5'-TCCCCTGAAGAAAATTGGTTAAAAT-3'; marmoset chorionic gonadotropin (*mCG*) β, 5'-CCCTGTGTGTCGCCTTT-3' and 5'-CTAATGGAGGGTCTGCTGGC-3'; *Bex1/Rex3*, 5'-ACAGGCAAGGATGAGAGAAG-3' and 5'-CCCACGTAAACAAGTGACAG-3'; HEB, 5'-ACTGAAACAAAGAAAGGATGAAAACC-3' and 5'-CCCTTTCTATCTTCTGTTCAGGGTTC-3'; *gp130*, 5'-AAACAGAACAGCATCCAGTC-3'and5'-AGTTGAGGCATCTTTGGTCC-3'; leukemia inhibitory factor receptor (LIFR), 5'-TTTCTTGGCATTTACCAGG-3' and 5'-GCTATTTTGGAAGGTGGTG-3'; β-*actin*, 5'-TCCTGACCCTSAAGTACCCC-3'and5'-GTGGTGGTGAAGCTGTAGCC-3'. Except for *CD34*, α-*fetoprotein*, and *mCG*, the expected sizes of the PCR products were estimated from human sequences. The expected PCR products were ~190 bp (*nanog*), ~530 bp (*oct3/4*), ~200 bp (*Sox-2*), ~356 bp (*FoxD3*), ~200 bp (*nestin*), 627 bp (*CD34*), 200 bp (α-*fetoprotein*), ~559 bp (*gp130*), ~269 bp (*Bex1/Rex3*), ~165 bp (*HEB*), 286 bp (*mCG*), ~514 bp (*LIFR*), and 418 bp (β-*actin*). The PCR reaction mixture (25 μl) contained ×1 PCR buffer (10 mM Tris-HCl [pH 9.0], 1.5 mM $MgCl_2$, 50 mM KCl), 0.2 mM dNTP, 0.5 μM of each primer, and 2.5 U *Taq* polymerase. The amplification was performed for 35 cycles of denaturation at 95°C for 1 minute, annealing at 60°C for 30 seconds, and elongation at 72°C. Representative RT-PCR products for each gene were verified by DNA sequencing (data not shown).

Analysis of Differentiation Potency

EB Formation

To study EB formation, undifferentiated ESCs were removed from the MEF feeder layer, dissociated using 0.25% trypsin in PBS with 20% KSR and 1 mM $CaCl_2$, and cultured in bacterial Petri dishes for 10–21 days using DMEM supplemented with 10% FBS. The medium was changed every 2 days.

In Vivo Differentiation Analysis: Teratoma Formation

To examine teratoma formation in mice, between 1–5 × 10^6 CMESCs were injected subcutaneously into the abdomen of 5-week-old immunodeficient mice, NOD/shi-scid, IL-2Rγ^{null} (NOG) mice [11]. Four to eight weeks after the injection, tumors were resected from the mice. The resected tumors were fixed in buffered formaldehyde, embedded in paraffin blocks, and subjected to immunohistochemical and histological examinations.

In Vitro Differentiation

Neural Cells

Stromal PA6 cells were plated on 12-mm coverslips and grown to semiconfluence. On day 0, 5 × 10^4 ESCs were cocultured with the PA6 cells on coverslips in Glasgow's modified Eagle's medium (GMEM) supplemented with 10% KSR, 0.1 mM 2-ME, and 10^{-7} M ascorbate. For the first 10 days of coculture, the medium was changed every 2 days. On day 12, the medium was exchanged for GMEM plus N-2 supplement (Invitrogen) that contained 0.1 mM 2-ME and 10^{-7} M ascorbate, and the culture was continued until day 20. The cells were then fixed with 4% paraformaldehyde in PBS.

Hematopoietic Cells

CMESCs were differentiated into hematopoietic cells by EB formation in Iscove's modified Dulbecco's medium (Invitrogen) that contained 15% FBS, 200 μg/ml transferrin, 10 μg/ml insulin, 50 μg/ml ascorbic acid, and 0.45 mM monothioglycerol. The CMESCs (10^4 cells per 9-cm dish) were cultured without cytokines for 14–18 days and then subjected to hematopoietic colony assays. Hematopoietic colonies were examined by growing differentiated ESC-derived cells (10^5 cells) in Methocult GF$^+$ medium (StemCell Technologies, Vancouver, British Columbia, Canada, http://www.stemcell.com) according to the manufacturer's instructions. After 10–14 days, the colony-forming units (CFU) were counted, and cellular morphology was confirmed microscopically using May-Giemsa staining of cytospun samples.

Results

Establishment of CMESC Lines

The marmosets ovulated 10.7 ± 1.3 days (n = 70) after PGF2α administration. Our ovarian cycle control system made it possible to obtain fertilized eggs every 3 weeks from the same animals. Sixty immunosurgically isolated ICMs from 70 blastocysts (the ICM isolation rate was 85.7%) were plated on the irradiated MEF feeder layer, and 11 ICMs were cultured for more than 10 passages (18.3% derivation rate). To date, 3/11 ICM-derived cells have been cultured for more than 1 year. All ICM-derived cells showed flat, packed, and tight colony morphology and a high nucleus:cytoplasm ratio (Figs. 1A, 1B). The morphology of these derived cells was very similar to that of reported primate ESCs, including those from humans and from rhesus and cynomolgus monkeys [12–16]. It has been reported that primate ESCs exhibit spontaneous differentiation during culture and that leukemia inhibitory factor does not maintain the ESCs in the undifferentiated state [13, 14]. The common marmoset ICM-derived cell lines also showed low frequency of differentiation. However, most ICM-derived cells maintained undifferentiated morphology of the cells. It is known that the quality of FBS is critical to the maintenance of undifferentiated primate ESCs; different lots of FBS from the same manufacturer can vary in this respect. Therefore, the chemically defined serum-free supplement KSR was used for the establishment and culture of the marmoset ESCs. The CMESC colonies appeared more packed and tight when KSR was used in the culture; they were flatter in appearance when FBS was used in the medium. To maintain stem cells, the dissociation procedure for cynomolgus ESCs was adopted for subculture of the marmoset ICM-derived cells [14]. With this culture system, continuous cultures of CMESCs have been sustained for more than 1 year.

Characterization of Undifferentiated CMESC Lines

To confirm the undifferentiated status of the ICM-derived cells, all three lines (CMESC 20, 30, and 40) were examined for the expression of cell surface markers that are specific for undifferentiated ESCs. As shown in Figures 1C–1G, the ICM-derived cell lines showed alkaline phosphatase activity (Fig. 1C) and expressed SSEA-3 (Fig. 1E), SSEA-4 (Fig. 1F), TRA-1-60 (Fig. 1G), and TRA-1-81 (Fig. 1H) but not SSEA-1 (Fig. 1D). All three cell lines retained the normal 46, XX karyotype (Fig. 2) and telomerase (Fig. 3A) activity. These three ICM-derived cell lines also expressed *Nanog*, *Oct3/4*, *Sox2*, *gp130*, *mCG*, *HEB*, and *Bex1/Rex3* mRNA and low levels of *FoxD3* and *Nestin* mRNA (Fig. 4A). Conversely, *LIFR* mRNA was not detected by RT-PCR. All three lines showed identical expression patterns of the genes. Therefore, we believe that these cells are CMESCs. To compare the gene expression patterns of fresh ICMs and the ICM-derived cell lines, RT-PCR analysis was conducted using fresh ICMs. As a result, the expression of *Nanog*, *Oct3/4*, and *Sox2* mRNA was

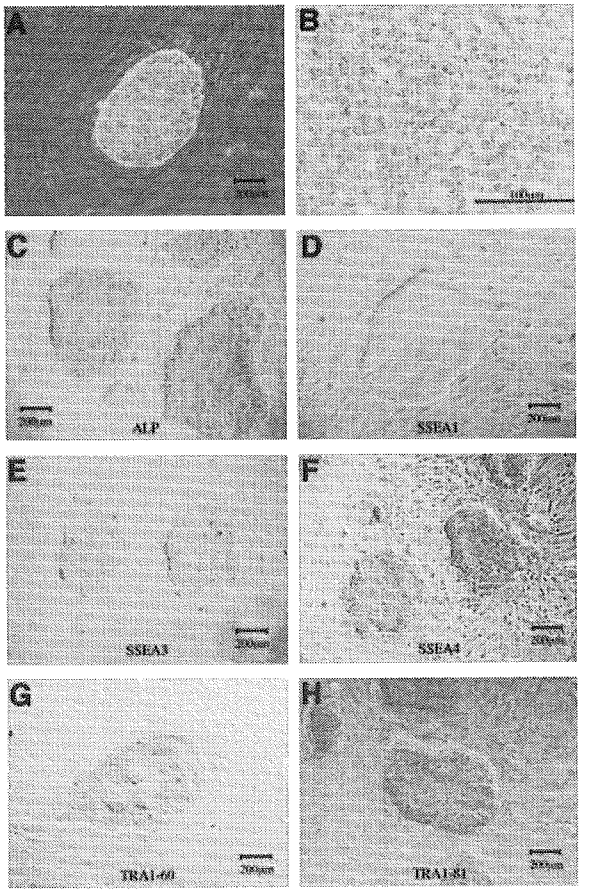

Figure 1. Expression of alkaline phosphatase and cell surface markers on CMESCs. Unstained CMESCs (**A, B**), cells stained for ALP (**C**), SSEA-1 (**D**), SSEA-3 (**E**), SSEA-4 (**F**), TRA-1-60 (**G**), and TRA-1-81 (**H**). Abbreviations: ALP, alkaline phosphatase; CMESC, common marmoset embryonic stem cell; SSEA, stage-specific embryonic antigen.

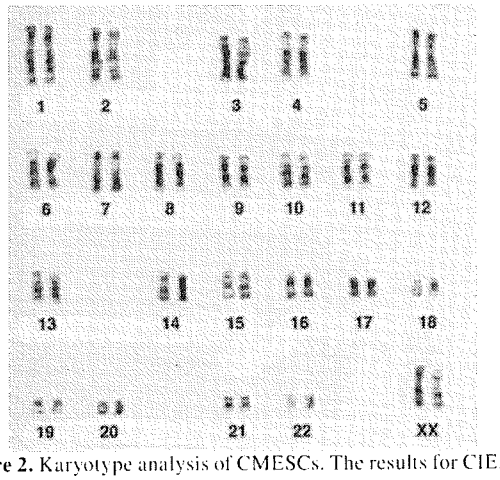

Figure 2. Karyotype analysis of CMESCs. The results for CIEA-CMESC #20 are shown. All three cell lines show the normal 46, XX karyotype after more than 6 months of culture. Abbreviations: CIEA, Central Institute for Experimental Animals; CMESC, common marmoset embryonic stem cell.

observed, whereas *FoxD3* and *Nestin* mRNA was not detected in fresh ICMs (Fig. 4B).

All three CMESC lines were examined for *MHC-DRB1* genotypes using PCR-based single strand conformation polymorphism (SSCP) methods. As shown in Figure 3B, the three CMESC lines were confirmed, based on different SSCP patterns, as having been established independently. Of these three CMESC lines, nos. 30 and 40 were derived from the same parents.

Differentiation Potency

Similar to other primate ESCs, CMESCs differentiate spontaneously during culturing on MEF feeder layer. However, the complete differentiation of CMESCs was suppressed by some growth factors or inhibitory factors from MEF feeder layer. To estimate the degree of differentiation, 50 CMESC clusters were seeded onto MEF feeder layer. As a result, 22%–74% ($n = 6$) of

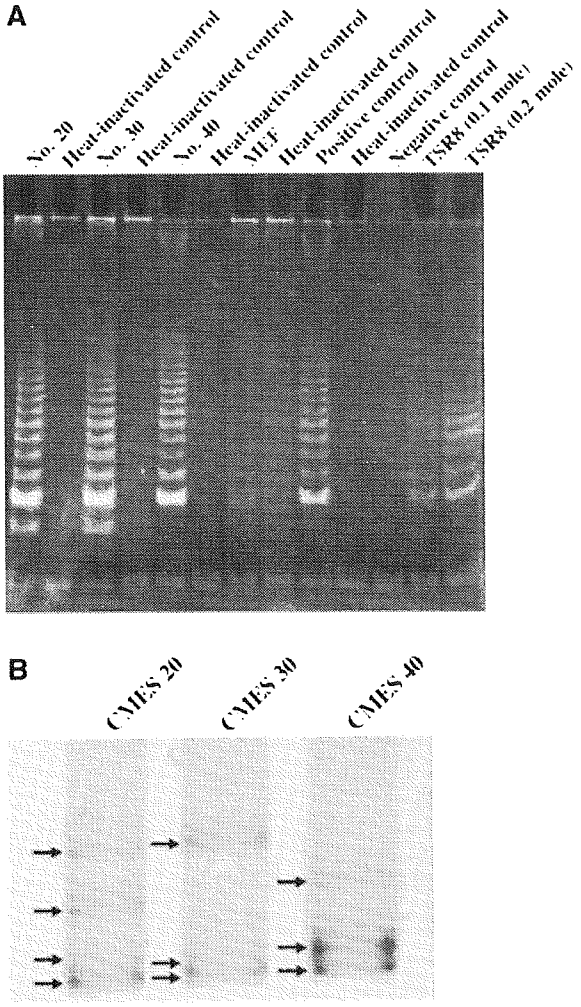

Figure 3. (A): Telomerase activities of CMESC lines. All three CMESC lines show high telomerase activity. On the other hand, MEF feeder layer does not show telomerase activity. **(B):** SSCP analysis of CMESCs for the *MHC-DRB1* gene. The results of SSCP indicate that all three lines were derived independently. Abbreviations: CMESC, common marmoset embryonic stem cell; MEF, mouse embryonic fibroblast; SSCP, single strand conformation polymorphism.

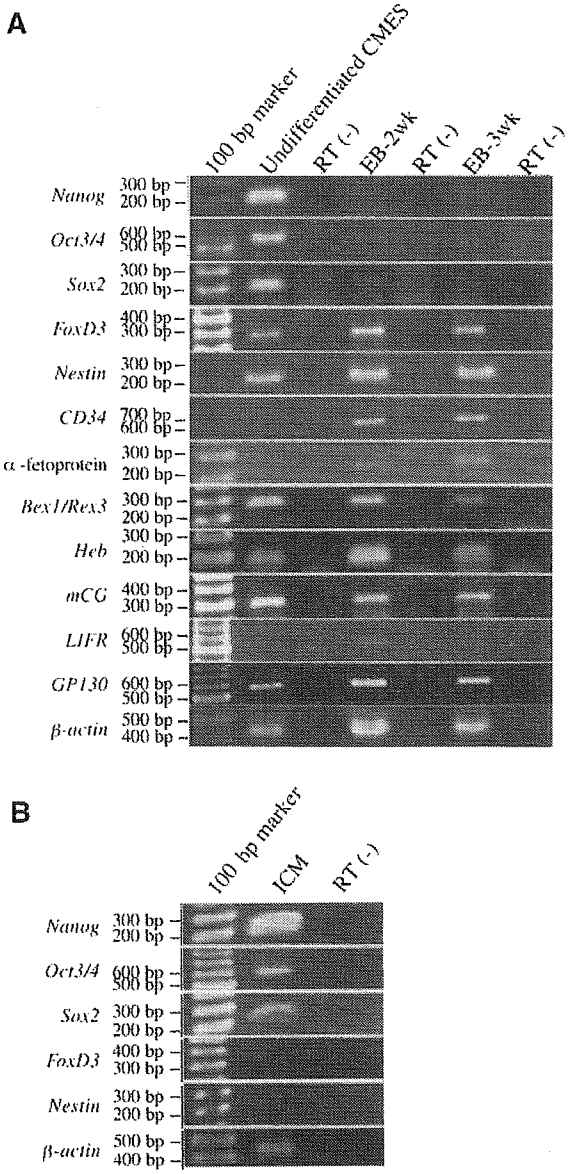

Figure 4. (A): RT-PCR analysis of CMESCs and EBs. Undifferentiated CMESCs expressed the *Nanog*, *Oct3/4*, *Sox2*, *FoxD3*, *Rex1/Rex3*, *Heb* and *mCG*, *GP130*, and low level of *Nestin* genes. Two-week cultures of EBs display expression of *Nestin* and *CD34*. Three-week cultures of EBs show expression of *Nestin*, *CD34*, and α-fetoprotein. *Oct3/4* and *Nanog* gene expression is shut down in the EBs. **(B):** RT-PCR analysis of fresh ICMs. ICMs expressed the *Nanog*, *Oct3/4*, and *Sox2* genes. Expression of *FoxD3* and *Nestin* was not detected. Abbreviations: CMESC, common marmoset embryonic stem cell; EB, embryoid body; ICM, inner cell mass; RT-PCR, reverse transcription–polymerase chain reaction.

the colonies (average 42.6%) were morphologically undifferentiated ESCs (data not shown). However, the differentiation rate of each cell was unclear because CMESCs need to be cell clusters to maintain undifferentiated status.

To assess the spontaneous differentiation potency of CMESCs, the formation of EBs and teratomas was examined. The suspension cultures of all three CMESC lines formed EBs (Figs. 5A, 5B). Simple EBs formed several days after the start of the suspension culture, and cystic EBs formed within 2 weeks. These EBs expressed mRNA for the *Nestin*, *CD34*, and α-fetoprotein genes, which are marker genes for the three germ layers, and *mCG*, *Bex1/Rex3*, and *Heb*, which are marker genes for trophectoderm (Fig. 4A). Furthermore, expression of *LIFR* and *gp130* was observed. However, *Nanog*, *Oct3/4*, and *Sox2* gene expression was shut off after 2 weeks of EB culture. In contrast, the expression level of *FoxD3* in EBs was greater than in undifferentiated CMESCs. To examine the differentiation potency in more detail, cells of CMESC 20 were injected subcutaneously into five immunodeficient NOG mice [11]. Eight weeks after injection, subcutaneous tumors were rescued from these mice and subjected to histological analysis. The tumor formation rate was 100% (5/5). The tumors were found to be teratomas that consisted of embryonic germ layers of ectodermal, mesodermal, and endodermal tissues (Figs. 6A–6M). Teratomas formed in all five NOG mice (100% teratoma formation rate). In the teratomas, the ectodermal tissue consisted of keratinized epidermis (Figs. 6B, 6G, and 7F) and neuronal cells (Fig. 6M); the mesodermal tissue was comprised of muscle (Figs. 6C, 6H) and blood vessels (Figs. 6I, 6J), and the endodermal tissue contained columnar epithelium (Figs. 6A, 6K, and 6L). Furthermore, cartilage-like tissue (Figs. 6A, 6D, and 6E) and adipose-like tissue (Fig. 6D) were also observed. These blood vessels were distinguished from murine blood vessels by immunohistochemical staining with human anti-CD31 antibody. Bronchus-like structures and gut-like structures were occasionally found in the teratomas (Figs. 6A, 6K, and 6L). Differentiation was confirmed by immunohistochemical analysis with several tissue-specific antibodies. As evidence for ESC differentiation into ectodermal cells, the GFAP-positive cells were observed as neuronal cells (Fig. 6M), and the keratinized epidermis-like structures in the teratomas expressed WSS keratin (Fig. 6G). The teratomas differentiated frequently into mesodermal tissues such as muscle, blood vessels, and cartilage. The muscle-like structure showed desmin expression, and CD31-positive cells were located in the hemangioendothelium of the blood vessel–like structures (Fig. 6J). The presence of the gut-like structures suggests endodermal differentiation. Alcian blue and periodic acid-Schiff (PAS) staining revealed mucus secretion from the columnar epithelium (Fig. 6L).

To investigate the in vitro differentiation potency of the CMESCs, the measurement of stromal cell–derived inducing activity (SDIA) was performed. After culture on PA6 cells for 20 days, extensive neurites appeared in the majority of the primate ESC colonies (67%, $n = 30$), which contained a large number of postmitotic neurons positive for class III β-tubulin (red; Fig. 7). SDIA has been reported to induce the production of tyrosine hydroxylase (TH)–positive dopaminergic neurons in mouse and

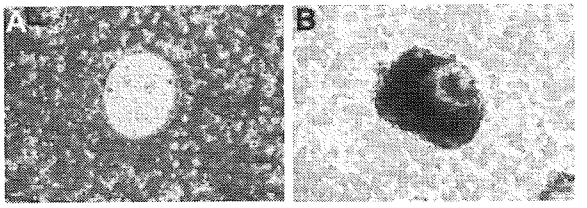

Figure 5. Spontaneous differentiation potency of CMESCs. A suspension culture of CMESCs shows the formation of EBs: **(A)** simple EB, **(B)** cystic EB. Abbreviations: CMESC, common marmoset embryonic stem cell; EB, embryoid body.

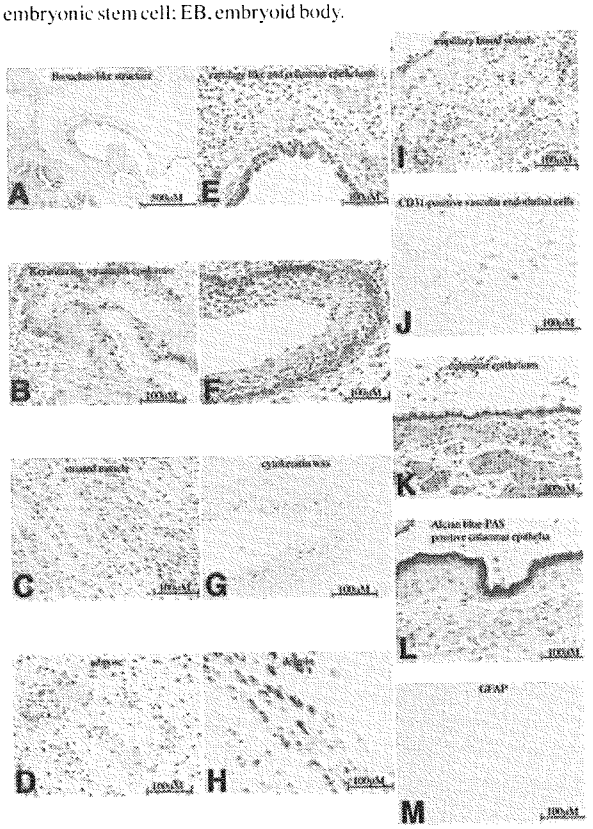

Figure 6. Differentiated CMESCs in teratomas and the expression of tissue-specific markers. **(A)**: A bronchus-like structure that consists of columnar epithelium surrounded by cartilage-like tissue. **(B–M)**: Keratinizing squamous epidermis **(B)**, striated muscle **(C)**, adipose-like tissue (high magnification) **(D)**, cartilage-like and columnar epithelium (high magnification) **(E)**, epidermis **(F)**, reactivity for cytokeratin WSS **(G)**, muscle-expressing desmin **(H)**, capillary blood vessels **(I)**, CD31-positive vascular endothelial cells **(J)**, columnar epithelium **(K)**, Alcian blue-PAS–positive columnar epithelia **(L)**, and GFAP-expressing neural cells **(M)**. Abbreviations: CMESC, common marmoset embryonic stem cell; GFAP, glial fibrillary acidic protein; PAS, periodic acid-Schiff; WSS, wide specific screening.

cynomolgus monkey ESCs and hESCs [17–19]. Therefore, we tested the marmoset cells for similar activities. After 2 weeks of induction, 14% of the class III β-tubulin–positive postmitotic neurons were TH-positive at the cellular level ($n = 50$). These cells were plated from trypsinized ESCs at passage. Most of the cells were derived from single cells, but only 15% of them expressed the TH protein. In the teratoma-like tumor induced by subcutaneous transplantation into NOG mice, some III β-tubulin–positive cells were found in colonies. Among III β-tublin–positive neurons, TH-positive neurons were found in 21% of them($n = 113$; data not shown).

To induce hematopoietic cells, EB formation was allowed to proceed in the cytokine-free medium, and CFU assays were performed. CFU-M (CFU-monocyte/macrophage) colonies were mainly observed under these conditions (Fig. 8A), and the main population of macrophages was confirmed microscopically using May-Giemsa staining of cytospun preparations (Fig. 8B).

Discussion

In this study, we have developed an embryo collection system that ensures a stable supply of common marmoset embryos for future production of transgenic or gene knockout marmosets. Our results show that marmoset ovulation is not disturbed, even after continuous administration of the PGF2α analogue cloprostenol. Thus, embryo collection from the same animal was carried out routinely, every 3 weeks, using cloprostenol administration. Using our embryo collection system, we recently established CMESC lines. In this study, we used a reported method of immunosurgery [9]. Although there was a high ICM isolation rate (85.7%) from blastocysts, the CMESC derivation rate was 18.3%, which is comparable to previous reports on other primate ESC lines, including 35.7% for human and 12.5% for cynomolgus monkey [14, 15]. The derivation rate of CMESC lines was considered to be dependent on the expansion procedure used for the cultured ICMs, including the in vitro developmental ability of embryos or the passage technique used for expanded ICMs.

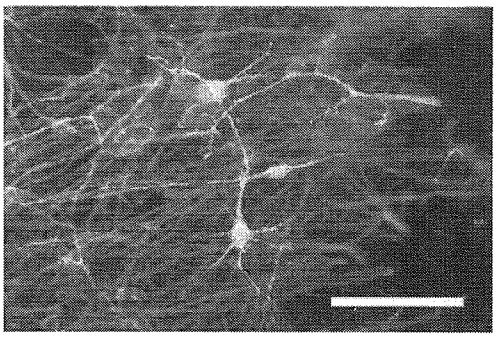

Figure 7. Neuronal cell differentiation of CMESCs in vitro. In vitro–differentiated ESCs using the SDIA method express TH protein and class III β-tubulin protein. Tyrosine hydroxylase: green; class III β-tubulin: red; Hoechst: blue. Scale bar = 80 mm. Abbreviations: CMESC, common marmoset embryonic stem cell; ESC, embryonic stem cell; SDIA, stromal cell–derived inducing activity.

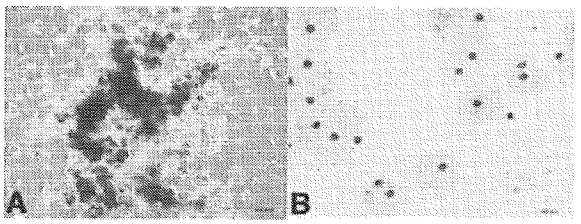

Figure 8. Hematopoietic CMESC differentiation in vivo. **(A):** CFU-M–like colonies predominate under these conditions. **(B):** May-Giemsa staining of colony-forming cells, confirming that the major population consists of macrophages. Abbreviations: CFU-M, colony-forming unit-monocyte/macrophage; CMESC, common marmoset embryonic stem cell.

The results of immunohistochemical analysis, enzymatic activity assays, RT-PCR analysis, and karyotype analysis show that the CMESC lines maintain their undifferentiated status. The RT-PCR results indicate that the gene expression patterns of undifferentiated CMESCs are similar to that of hESCs and different from those of mouse ESCs. In undifferentiated CMESCs, the expression patterns of *Oct3/4*, *Nanog*, *Sox2*, *mCG*, *HEB*, and *Bex1/REX3* gene mRNA were identical to hESCs or marmoset ESCs [6, 20]. In contrast, a very low level of *FoxD3* expression was observed in undifferentiated CMESCs. In fresh ICMs, the expression of *Nanog*, *Oct3/4*, and *Sox2* was observed, whereas that of *FoxD3* and *Nestin* was not. The presence of *Nanog*, *Oct3/4*, and *Sox2* mRNA expression in both fresh ICMs and CMESCs suggests that these genes are required to maintain stemness of cells in vitro and in vivo. Because *FoxD3* and *Nestin* were expressed at very low levels in undifferentiated CMESCs, it is possible that these genes in fresh ICMs are expressed under the detection level of our RT-PCR analysis. Another possibility is that the *FoxD3* and *Nestin* genes were amplified from spontaneously differentiated CMESCs in the cultured CMESCs. The latter possibility is supported by increased *FoxD3* gene expression in EBs. As the *FoxD3* gene expressed in murine undifferentiated ESCs [20], the different *FoxD3* expression patterns in primate and murine ESCs suggests that *FoxD3* plays a different role in respective ESCs. The expression of *mCG* and *Bex1/REX3* reflects the ability of CMESCs to differentiate into trophectodermal cells. These results match the ability of other primate ESCs to differentiate into trophectodermal cells.

The molecular mechanisms that maintain undifferentiated primate ESCs are largely unknown, and MEF feeder layer is essential to maintain undifferentiated primate ESCs. CMESCs also differentiated spontaneously on MEF feeder layer at low frequency. The expression of *gp130* and the absence of *LIFR* in CMESCs were identical to hESCs. These results indicate that maintaining undifferentiated CMESCs is not dependent on LIF signals. However, the expression of *gp130* suggested that other gp130-STAT3 signals, such as interleukin (IL)-6, oncostatin M,

or IL-11, play a role in CMESC proliferation or differentiation. The MEF feeder layer dependency of primate ESCs is considered one significant obstacle to using hESCs for stem therapy. Elucidation of the molecular mechanisms for the maintenance or development of MEF feeder layer–free culture systems of undifferentiated primate ESCs is one of the important themes of ESC research. Combined, these results suggest that the cellular characteristics and activities of CMESCs are similar to those of human and other primate ESCs [6, 12–16, 21, 22].

The spontaneous differentiation abilities of the CMESCs were verified by EB formation (Fig. 5) and teratoma formation (Fig. 6). RT-PCR analysis of EBs showed that the CMESCs differentiated into three germ layers in vitro. Furthermore, when the CMESCs were transplanted subcutaneously into immunodeficient NOG mice, teratomas that consisted of three-dimensional tissue structures were formed with high efficiency (100%). When SCID mice were used for the teratoma formation experiment, the teratoma formation rate was also 100% (two of two NOD/SCID mice, data not shown). Therefore, the formation of teratomas indicates that CMESCs have multipotent differentiation ability. The teratomas were also examined by immunohistochemistry, using several tissue-specific antibodies. The most frequently observed tissue type in the teratomas was mesodermal, which included cartilage (Figs. 6A, 6D, and 6E), muscle (Figs. 6C, 6H), and blood vessels (Fig. 6I). Although the frequency of endodermal tissue differentiation was lower than the frequencies of ectodermal and mesodermal tissue differentiation, endodermal tissue differentiation was clearly demonstrated with one of our CMESC lines (no. 20). Interestingly, Alcian blue and PAS staining of columnar epithelium showed the secretion of mucus from the cells, which indicates that CMESCs can differentiate into functional endodermal cells (Fig. 6L). Teratoma formation was not demonstrated for the marmoset ESC line (cj 11) established by Thomson et al. [6]. Both CMESC and cj 11 showed similar morphology and identical marker expression patterns. However, when we examined teratoma formation with a marmoset ESC line purchased from the WiCell Research Institute, Inc. (Madison, WI, http://www.wicell.org), we obtained fibrosarcomas, but no teratomas, in NOD/SCID mice (data not shown). The reasons for successful in vivo teratoma formation with our ESCs remain to be elucidated.

SDIA caused CMESC lines 20 and 40 to differentiate into TH-positive neurons in vitro (Fig. 7). In vitro differentiation into hematopoietic cells from EBs was measured in colony assays. Although other types of hematopoietic colonies were not seen in all experiments ($n > 7$), other conditions, such as gene-transfer methods, make it possible to induce various hematopoietic colonies from CMESCs (Kurita et al., personal communication), which suggests that CMESCs have the ability to differentiate into multiple hematopoietic lineages. These results support our finding that CMESCs have the capacity to differentiate into functional cells both in vitro and in vivo. Therefore, CMESCs can be used in preclinical studies aimed at developing regenerative medicines.

In this study, the teratoma formation and in vitro differentiation experiments show the strong differentiating potency of our CMESC lines; in addition, this is the first report to demonstrate the pluripotency of CMESCs. Our pluripotent CMESC lines should be very useful in establishing a preclinical animal model system for predicting the safety and efficacy of regenerative therapies using hESCs. Chimerism and the germ line transmission ability of CMESCs are not yet known. The mechanisms of the germ line transmission of ESCs are unknown, and in primates and other mammals, except mice, germ line transmission of ESCs has not been reported. Therefore, it is possible that germ line transmission of CMESCs will not occur in chimeras. If CMESCs do not transmit into the germ line, somatic cell nuclear transfer from the chimera or gametogenesis from CMESCs is one way to solve the problem [23–25].

Recently, various types of cells differentiated from hESCs or nonhuman ESCs have been reported [18, 26–36]. For example, hematopoietic cells, dopaminergic neurons, and insulin-producing cells have been generated from hESCs or primate ESCs. However, reports of transplantation of these differentiated ESCs into nonhuman primates are very rare [37]. There are various difficulties involved in using nonhuman primates as experimental animals. For example, rhesus or cynomolgus monkeys in which the ESC line has already been established are too expensive and cumbersome. Furthermore, immunological incompatibility between ESCs and animals may represent a significant obstacle to ESC transplantation. Taking this situation into consideration, the common marmoset has advantages, such as low cost and ease of maintenance. Importantly, marmosets are immunogenetically closed because they have been bred in large closed colonies. Thus, the common marmoset and CMESCs provide an excellent experimental model system for studies into the mechanism of cell differentiation, as well as for the development of regenerative therapies using hESCs.

Acknowledgments

We thank Dr. Sumiko Watanabe, Dr. Chieko Kai, and Dr. Ken-ichi Arai for very helpful advice and persistent support. This work was supported by grants from the Japan Society for the Promotion of Science and Research for the Future Program and partially by the Ministry of Education, Culture, Sports, Science, and Technology.

Disclosures

The authors indicate no potential conflicts of interest.

References

1 Lopata A, Summers PM, Hearn JP. Births following the transfer of cultured embryos obtained by in vitro and in vivo fertilization in the marmoset monkey (*Callithrix jacchus*). Fertil Steril 1988;50:503–509.

2 Summers PM, Shephard AM, Taylor CT et al. The effects of cryopreservation and transfer on embryonic development in the common marmoset monkey, *Callithrix jacchus*. J Reprod Fertil 1987;79:241–250.

3 Marshall VS, Kalishman J, Thomson JA. Nonsurgical embryo transfer in the common marmoset monkey. J Med Primatol 1997;26:241–247.

4 Hibino H, Tani K, Ikebuchi K et al. The common marmoset as a target preclinical primate model for cytokine and gene therapy studies. Blood 1999;93:2839–2848.

5 Mansfield K. Marmoset models commonly used in biomedical research. Comp Med 2003;53:383–392.

6 Thomson JA, Kalishman J, Golos TG et al. Pluripotent cell lines derived from common marmoset (*Callithrix jacchus*) blastocysts. Biol Reprod 1996;55:254–259.

7 Summers PM, Wennink CJ, Hodges JK. Cloprostenol-induced luteolysis in the marmoset monkey (*Callithrix jacchus*). J Reprod Fertil 1985;73:133–138.

8 Harlow CR, Gems S, Hearn JP et al. The relationship between plasma progesterone and the timing of ovulation and early embryonic development in the marmoset monkey (*Callithrix jacchus*). J Zool 1983;201:273–282.

9 Solter D, Knowles BB. Immunosurgery of mouse blastocyst. Proc Natl Acad Sci U S A 1975;72:5099–5102.

10 Wu MS, Tani K, Sugiyama H et al. MHC (major histocompatibility complex)-DRB genes and polymorphisms in common marmoset. J Mol Evol 2000;51:214–222.

11 Ito M, Hiramatsu H, Kobayashi K et al. NOD/SCID/gamma(c)(null) mouse: an excellent recipient mouse model for engraftment of human cells. Blood 2002;100:3175–3182.

12 Thomson JA, Kalishman J, Golos TG et al. Isolation of a primate embryonic stem cell line. Proc Natl Acad Sci U S A 1995;92:7844–7848.

13 Reubinoff BE, Pera MF, Fong CY et al. Embryonic stem cell lines from human blastocysts: somatic differentiation in vitro. Nat Biotechnol 2000;18:399–404.

14 Suemori H, Tada T, Torii R et al. Establishment of embryonic stem cell lines from cynomolgus monkey blastocysts produced by IVF or ICSI. Dev Dyn 2001;222:273–279.

15 Thomson JA, Itskovitz-Eldor J, Shapiro SS et al. Embryonic stem cell lines derived from human blastocysts. Science 1998;282:1145–1147.

16 Mitalipova M, Calhoun J, Shin S et al. Human embryonic stem cell lines derived from discarded embryos. STEM CELLS 2003;21:521–526.

17 Kawasaki H, Mizuseki K, Nishikawa S et al. Induction of midbrain dopaminergic neurons from ES cells by stromal cell-derived inducing activity. Neuron 2000;28:31–40.

18 Kawasaki H, Suemori H, Mizuseki K et al. Generation of dopaminergic neurons and pigmented epithelia from primate ES cells by stromal cell-derived inducing activity. Proc Natl Acad Sci U S A 2002;99:1580–1585.

19 Perrier AL, Tabar V, Barberi T et al. Derivation of midbrain dopamine neurons from human embryonic stem cells. Proc Natl Acad Sci U S A 2004;101:12543–12548.

20 Ginis I, Luo Y, Miura T et al. Differences between human and mouse embryonic stem cells. Dev Biol 2004;269:360–380.

21 Stojkovic M, Lako M, Stojkovic P et al. Derivation of human embryonic stem cells from day-8 blastocysts recovered after three-step in vitro culture. STEM CELLS 2004;22:790–797.

22 Stojkovic M, Lako M, Strachan T et al. Derivation, growth and applications of human embryonic stem cells. Reproduction 2004;128:259–267.

23 Toyooka Y, Tsunekawa N, Akasu R et al. Embryonic stem cells can form germ cells in vitro. Proc Natl Acad Sci U S A 2003;100:11457–11462.

24 Hubner K, Fuhrmann G, Christenson LK et al. Derivation of oocytes from mouse embryonic stem cells. Science 2003;300:1251–1256.

25 Simerly C, Navara C, Hyun SH et al. Embryogenesis and blastocyst development after somatic cell nuclear transfer in nonhuman primates: overcoming defects caused by meiotic spindle extraction. Dev Biol 2004;276:237–252.

26 Assady S, Maor G, Amit M et al. Insulin production by human embryonic stem cells. Diabetes 2001;50:1691–1697.

27 Schuldiner M, Eiges R, Eden A et al. Induced neuronal differentiation of human embryonic stem cells. Brain Res 2001;913:201–205.

28 Kaufman DS, Hanson ET, Lewis RL et al. Hematopoietic colony-forming cells derived from human embryonic stem cells. Proc Natl Acad Sci U S A 2001;98:10716–10721.

29 Kehat I, Kenyagin-Karsenti D, Snir M et al. Human embryonic stem cells can differentiate into myocytes with structural and functional properties of cardiomyocytes. J Clin Invest 2001;108:407–414.

30 Umeda K, Heike T, Yoshimoto M et al. Development of primitive and definitive hematopoiesis from nonhuman primate embryonic stem cells in vitro. Development 2004;131:1869–1879.

31 Haruta M, Sasai Y, Kawasaki H et al. In vitro and in vivo characterization of pigment epithelial cells differentiated from primate embryonic stem cells. Invest Ophthalmol Vis Sci 2004;45:1020–1025.

32 Mizuseki K, Sakamoto T, Watanabe K et al. Generation of neural crest-derived peripheral neurons and floor plate cells from mouse and primate embryonic stem cells. Proc Natl Acad Sci U S A 2003;100:5828–5833.

33 Kuo HC, Pau KY, Yeoman RR et al. Differentiation of monkey embryonic stem cells into neural lineages. Biol Reprod 2003;68:1727–1735.

34 Calhoun JD, Lambert NA, Mitalipova MM et al. Differentiation of rhesus embryonic stem cells to neural progenitors and neurons. Biochem Biophys Res Commun 2003;306:191–197.

35 Lang KJ, Rathjen J, Vassilieva S et al. Differentiation of embryonic stem cells to a neural fate: a route to re-building the nervous system? J Neurosci Res 2004;76:184–192.

36 Li F, Lu S, Vida L et al. Bone morphogenetic protein 4 induces efficient hematopoietic differentiation of rhesus monkey embryonic stem cells in vitro. Blood 2001;98:335–342.

37 Nara Y, Muramatsu S, Nakano I. ES cell therapy for Parkinson's disease. Nippon Rinsho 2004;62:1643–1647.

Midterm Results on Ocular Surface Reconstruction Using Cultivated Autologous Oral Mucosal Epithelial Transplantation

TSUTOMU INATOMI, MD, PHD, TAKAHIRO NAKAMURA, MD, PHD, NORIKO KOIZUMI, MD, PHD, CHIE SOTOZONO, MD, PHD, NORIHIKO YOKOI, MD, PHD, AND SHIGERU KINOSHITA, MD, PHD

• PURPOSE: To perform a midterm assessment of the integrity and reproducibility of cultivated autologous oral mucosal epithelial sheets, and to evaluate the clinical efficacy of their transplantation in ocular surface.
• DESIGN: Observational case series.
• METHODS: Cultivated autologous oral mucosal epithelial sheets were created using amniotic membrane and buccal mucosal epithelium from 12 patients with Stevens-Johnson syndrome, chemical and thermal injury, pseudo-ocular cicatricial pemphigoid, and idiopathic ocular surface disorder. They were transplanted onto 15 eyes from these patients who were then followed up for a mean of 20 months; with the longest follow-up being 34 months. We assessed their clinical outcomes with special reference to neovascularization.
• RESULTS: Cultivated autologous oral mucosal epithelial sheets could be generated from all patients. On the second postoperative day, 14 of 15 sheets transplanted demonstrated total re-epithelialization on the cornea. During the follow-up, the ocular surface was stable and transparent without any major complications in 10 of 15 eyes (67%), and the transplanted epithelium survived for at least 34 months. There were five eyes (33%) with small but long-standing epithelial defects, three of these healed spontaneously, and two (13%) required reoperation. In 10 eyes, postoperative visual acuity was improved by more than 2 lines. All eyes manifested some peripheral corneal vascularization.
• CONCLUSIONS: We established a successful tissue-engineering technique to generate cultivated autologous oral mucosal epithelial sheets and succeeded in reconstructing the ocular surface. We suggest that this surgical modality may be both safe and useful, especially in younger patients with the most severe ocular surface disorders. (Am J Ophthalmol 2006;141:267–275. © 2006 by Elsevier Inc. All rights reserved.)

See accompanying Editorial on page 356.
Accepted for publication Sep 2, 2005.
From the Department of Ophthalmology, Kyoto Prefectural University of Medicine, Kyoto, Japan.
Supported in part by Grants-in-Aid for translational research and scientific research from the Japanese Ministry of Education, Culture, Sports, Science and Technology, Grants from the Japanese Ministry of Health, Labor and Welfare, and a research grant from the Kyoto Foundation for the Promotion of Medical Science.
Inquiries to Shigeru Kinoshita, MD, PHD, Department of Ophthalmology, Kyoto Prefectural University of Medicine, Kawaramachi Hirokoji, Kamigyo-ku, Kyoto 602-0841 Japan; fax: +81-75-251-5663; e-mail: shigeruk@ophth.kpu-m.ac.jp

THE COMPLETE LOSS OF CORNEAL EPITHELIAL STEM cells attributable to acute or chronic ocular surface disorders leads to limbal deficiency that results in the conjunctivalization of the corneal surface, that is, conjunctival epithelial invasion with superficial vascularization and subepithelial scarring. Various degrees of pathologic keratinization, symblepharon, and entropion also occur, resulting in serious visual loss. Surgical approaches to ocular surface diseases such as Stevens-Johnson syndrome (SJS), ocular cicatricial pemphigoid, and chemical injury include limbal transplantation[1] and amniotic membrane (AM) transplantation.[2] These approaches were both developed in the 1990s and have produced some positive therapeutic results.

The more recently developed and improved surgical modality that uses cultivated corneal epithelial stem cell sheets has already been implemented widely.[3–7] The primary concept and cultivation technique for epithelium is an extension of the method first introduced in the 1970s by Rheinwald and Green[8] that employed tissue-engineered epidermal sheets to treat thermal skin injuries.

Despite a number of failures, in part attributable to a lack of knowledge regarding stem cells, in 1997 Pellegrini and associates[9] successfully restored damaged human corneal surfaces by transplanting autologous cultivated corneal epithelium. Subsequently, patients with unilateral damage received transplants of cultivated corneal epithelial stem cells obtained from the healthy contralateral eye. This has become an established, successful approach.[3,10,11] Patients with bilateral eye damage required the transplantation of cultivated corneal epithelial stem cells from

0002-9394/06/$32.00
doi:10.1016/j.ajo.2005.09.003

TABLE 1. Baseline Data of Patients Receiving an Oral Mucosal Epithelial Culture Reconstruction

Case	Age/Gender	Disease	Condition of Oral Cavity	Feeder Cell Condition	Culture Serum	Density of Cell Seeding (Cell/Well)	Days Reach Confluence	Integrity of Culture Sheet
1	33/M	Chemical	Good	Good	FBS	1.0×10^5	5	Excellent
2	33/M	Chemical	Good	Good	FBS	1.0×10^5	5	Excellent
3	27/M	Chemical	Good	Good	FBS	1.0×10^5	6	Excellent
4	24/M	SJS	Moderate	Good	FBS	0.9×10^5	6	Excellent
5	14/F	SJS	Moderate	Good	FBS	0.7×10^5	6	Excellent
6	24/M	SJS	Moderate	Good	FBS	1.1×10^5	8	Excellent
7	65/F	SJS	Moderate	Good	FBS	0.7×10^5	6	Fair
8	61/F	OSD	Good	Moderate	FBS	1.0×10^5	7	Excellent
9	69/M	Chemical	Good	Good	FBS	1.0×10^5	6	Excellent
10	65/F	SJS	Moderate	Good	AS	1.5×10^5	7	Excellent
11	70/M	SJS	Moderate	Good	AS	1.3×10^5	6	Excellent
12	67/F	SJS	Moderate	Good	AS	1.5×10^5	6	Excellent
13	29/M	Thermal	Moderate	Good	AS	1.0×10^5	5	Excellent
14	81/F	pOCP	Good	Good	AS	1.5×10^5	6	Excellent
15	64/M	Chemical	Moderate	Good	AS	1.5×10^5	7	Excellent

AS = autologous serum; Chemical = chemical injury; FBS = fetal bovine serum; OSD = idiopathic ocular surface disorder; pOCP = pseudo-ocular cicatricial pemphigoid; SJS = Stevens-Johnson syndrome; Thermal = thermal injury.

cadaver donors or a living-related eye. While this method also yielded some success,[4,12] immunologic rejection and microbial infection as a result of immunosuppressive therapy after allogeneic transplantation continue to present challenges.

In the context of regenerative medicine, the transplantation of cultivated mucosal epithelial stem cell sheets created from autologous cell sources presents a viable alternative in cases with bilateral eye damage that vitiates the use of autologous corneal epithelial stem cells. Oral mucosal epithelium has attracted attention as a cell source, and favorable results have been obtained in animal- and preliminary human pilot studies.[13-16]

Here we present midterm clinical data on 15 eyes grafted with cultivated autologous oral mucosal epithelial transplants. The corneal surface in 13 of our 15 eyes was stable and remained fairly transparent despite some peripheral corneal neovascularization.

METHODS

THIS STUDY WAS APPROVED BY THE INSTITUTIONAL REview Board for Human Studies of Kyoto Prefectural University of Medicine; prior informed consent was obtained from all patients. We report on 15 eyes from 12 patients with bilateral total limbal deficiency; their ages ranged from 14 to 81 years. The preoperative diagnosis was SJS in five patients, chemical injury in four, and thermal injury, pseudo-ocular cicatricial pemphigoid, and idiopathic ocular surface disorder of unknown etiology in one patient each. Preoperatively, all 15 eyes manifested severe destruction of the ocular surface with limbal deficiency, but also reasonable reflex tearing with some meniscus height.

The 12 patients presented displayed total limbal deficiency in either the acute or chronic phase. This was diagnosed by the complete absence of the palisades of Vogt. The four eyes in the acute phase had sustained chemical (n = 3) or thermal injury (n = 1) and manifested persistent epithelial defects involving the entire cornea, complete limbal deficiency, and sustained conjunctival inflammation. The injury to these four eyes was of grade IIIb or IV according to the grading system we proposed elsewhere.[17] The 11 eyes in the chronic phase included seven with SJS, two with chemical injuries, and one each with pseudo-ocular cicatricial pemphigoid and idiopathic ocular surface disorder. All 11 eyes manifested total conjunctivalization on the cornea with conjunctival cicatrization. Of the 15 eyes, seven had received previous treatment consisting of AM transplantation alone (n = 2), limbal transplantation with AM transplantation (n = 1), keratoepithelioplasty with AM transplantation (n = 1), and penetrating keratoplasty (n = 1); both eyes in one patient had been grafted with cultivated allogeneic corneal epithelial sheets in the acute phase. The mean follow-up period in our midterm study was 20 months; the longest follow-up was 34 months.

● PROCEDURE FOR THE TISSUE-ENGINEERING OF AUTOLOGOUS ORAL MUCOSAL EPITHELIAL SHEETS: After obtaining informed consent in accordance with the tenets of the Declaration of Helsinki for research involving human subjects, we harvested human AM at the time of elective Cesarean section. Under sterile conditions, the membranes were deprived of their amniotic epithelium by

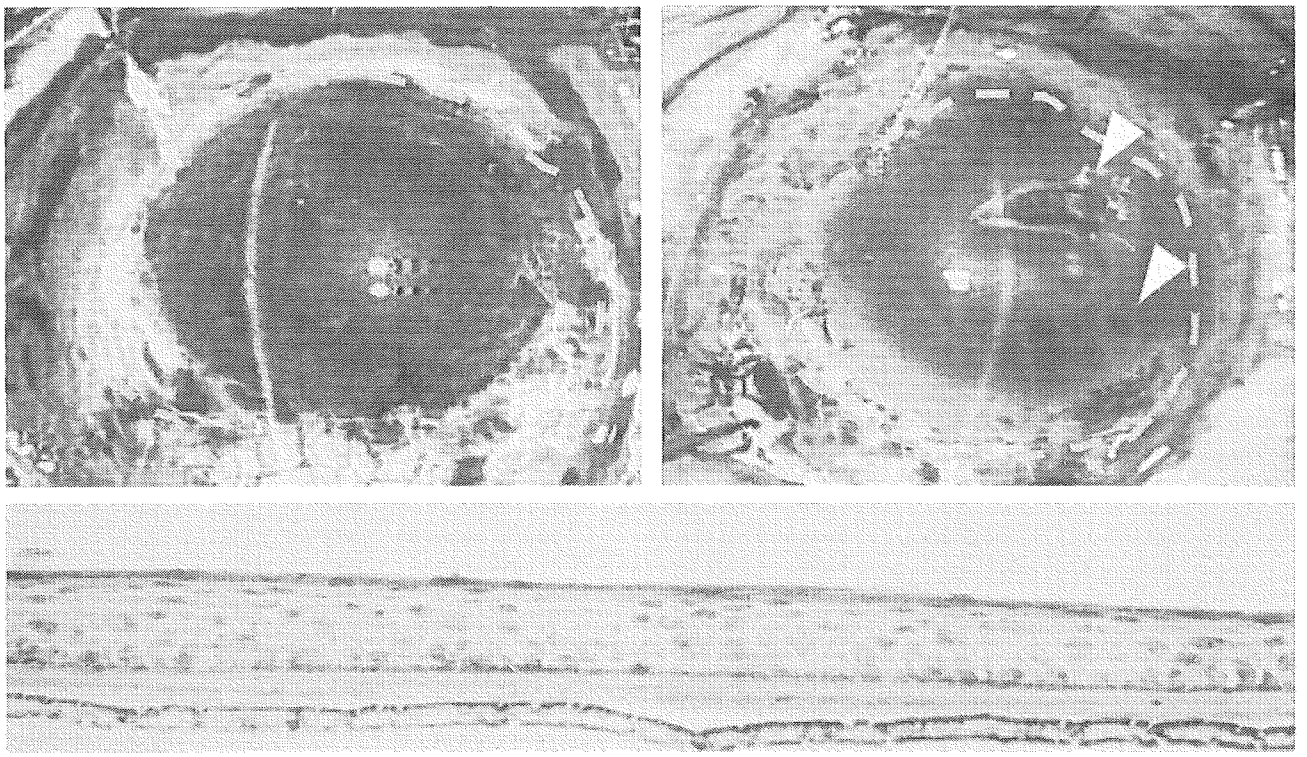

FIGURE 1. The integrity of all transplanted cultivated oral mucosal epithelial sheets confirmed by fluorescein staining at the end of ocular surface reconstruction. The yellow broken line encompasses negatively-stained cultivated stratified oral mucosal epithelium. Arrows indicate the region harboring the epithelial defect in the sheet that was considered to be of only fair quality before grafting. Of the 15 sheets, 14 (93.3%) were of excellent quality and without epithelial defects (Top left); one case was scored as fair with some epithelial defects (Top right). Histologic examination using hematoxylin and eosin staining revealed good stratification throughout the entire sheet (Bottom). EP: cultivated oral mucosal epithelium; AM: amniotic membrane; CI: culture insert.

using a 2-hour incubation at 37°C with ethylene diamine tetraacetic acid (EDTA) 0.02% to loosen cell adhesion. This was followed by gentle scraping with a cell scraper.

The presence of healthy oral mucosa in our patients was confirmed by a dentist before biopsy. All patients were monitored to confirm their adherence to required tooth-decay treatment, their abstinence from alcohol or tobacco use, and their regular performance of tooth brushing and iodine gargling. Under local anesthesia, oral mucosal biopsy specimens, each measuring approximately 2 to 3 mm^2, were obtained 2 to 3 weeks before the planned transplantation procedure. Submucosal connective tissues were removed with scissors to the extent possible, with the resulting samples being cut into small explants that were then immersed three times (10 minutes, room temperature) in phosphate-buffered saline solution containing antibiotics (50 IU/ml penicillin-streptomycin and 5 μg/ml amphotericin B). The explants were then incubated at 37°C for 1 hour with 1.2 IU dispase as previously described[13] and treated with trypsin-EDTA 0.05% solution for 10 minutes at room temperature to separate the cells. Enzyme activity was stopped by washing with culture medium comprised of DMEM and Ham's F12 medium (1:1) containing insulin (5 μg/ml), cholera toxin (0.1 nmol/l), human recombinant epidermal growth factor (10 ng/ml), and penicillin-streptomycin (50 IU/ml). In cultures for eyes no. 1 to 9, the medium also contained 10% fetal calf serum. In cultures for eyes no. 10 to 15, we included 10% autologous serum. The oral mucosal epithelium was then seeded onto denuded AM spread on the bottom of culture inserts, and cocultured with mitomycin-C (MMC)-inactivated 3T3 fibroblasts. The culture was submerged in medium for 2 weeks and then exposed to air by lowering the level of the medium (air lifting) for 1 to 2 days. Cultures were incubated at 37°C in a 5% CO_2-95% air incubator; the medium being changed daily. Baseline data on the oral mucosal epithelial cultures are summarized in Table 1.

• SURGICAL PROCEDURE FOR OCULAR SURFACE RECONSTRUCTION USING CULTIVATED AUTOLOGOUS ORAL MUCOSAL EPITHELIAL TRANSPLANTATION: The surgical procedure was as described in our previous report.[4] Stated briefly, after a 360-degree conjunctival peritomy, we either scraped the area with the epithelial defect, or completely removed the conjunctivalized tissue by thin superficial keratectomy on the corneal surface. Subconjunctival spaces were treated with MMC 0.04% for 5 minutes, followed by a vigorous washing with saline. Then,

TABLE 2. Characteristics of Cases and Clinical Outcome of Patients With Oral Mucosal Epithelial Culture Reconstruction

Case	Age/Gender	Eye	Disease	Prior Op	Combined Op	Visual Acuity			Complication	Follow-up (mos)
						Pre Op	Post Op	Last VA		
1	33/M	OS	Chemical (acute)	AMT		HM	20/200	20/40		34
2	33/M	OD	Chemical (acute)	AMT		HM	HM	HM		34
3	27/M	OS	Chemical (chronic)	None	AMT	HM	CF	HM		32
4	24/M	OS	SJS	CCET		HM	20/2000	CF	ED	29
5	14/F	OS	SJS	None		CF	20/1000	20/1000		28
6	24/M	OD	SJS	CCET		HM	20/2000	CF	ED	28
7	65/F	OD	SJS	AMT + KEP	PEA + IOL	CF	20/400	20/500	ED	26
8	61/F	OD	OSD	AMT + LT	PEA + IOL	HM	20/500	20/800		23
9	69/M	OD	Chemical (chronic)	PK	PK*	HM	HM	20/50		18
10	65/F	OS	SJS	None	PEA + IOL	HM	20/320	20/320		12
11	70/M	OS	SJS	None	PK*	HM	HM	20/1000		11
12	67/F	OD	SJS	None	PEA + IOL	HM	20/2000	20/2000	ED	8
13	29/M	OD	Thermal (acute)	None	Lid	20/500	20/1000	20/32	ED	8
14	81/F	OS	pOCP	None	PEA + IOL + PPV	20/400	20/63	20/63		6
15	64/M	OD	Chemical (acute)	None	PEA + IOL + Lid	20/500	20/250	20/500		3

AMT = amniotic membrane transplantation; CCET = cultivated corneal epithelial transplantation; CF = count finger; Chemical = chemical injury; ED = epithelial defect; HM = hand motion; IOL = intraocular lens; KEP = keratoepithelioplasty; Lid = lid plastic surgery; LT = limbal transplantation; OSD = idiopathic ocular surface disorder; PEA = phacoemulsification; PK = penetrating keratoplasty; pOCP = pseudo-ocular cicatricial pemphigoid; PPV = pars plana vitrectomy; SJS = Stevens-Johnson syndrome; Thermal = thermal injury.
*Two cases received PK after primary surgery.

the cultivated autologous oral mucosal epithelial sheet in a culture dish was cut with a 19-mm diameter trephine, transferred onto the corneal surface, and sutured with 10-0 nylon. The integrity of the cultivated epithelium was confirmed by fluorescein staining at the end of surgery (Figure 1), and the ocular surface was protected with a medical-use contact lens.

• CLINICAL EVALUATION: Preoperative and postoperative best-corrected visual acuity was measured, and ocular surface manifestations were inspected with a slit-lamp microscope and fluorescein staining. Corneal superficial vascularization was monitored photographically and graded according to extent and intensity, where grade 1 indicates peripheral vascularization, grade 2 peripheral and midperipheral vascularization, grade 3 modest vascularization involving the entire cornea, and grade 4 massive vascularization of the entire cornea.

RESULTS

• CULTIVATED AUTOLOGOUS ORAL MUCOSAL EPITHELIAL SHEETS: There were no complications during or after the excision of oral mucosa. Cell suspensions of approximately 1×10^5 seeded oral mucosal epithelial cells began to form colonies on the denuded AM within 3 days. After 5 to 8 days in culture, a confluent primary culture of oral mucosal epithelial cells was established on the whole AM. After 2 weeks, the cultivated oral mucosal epithelium consisted of five to six cell layers and was similar to the cultivated corneal epithelial sheets we reported previously.[4,13] The oral mucosal epithelial sheet was composed of a well-conserved basal layer formed by cuboidal cells, several suprabasal cell layers, and flat apical cell layers (Figure 1). In 14 of 15 instances, the quality of the cultivated epithelial sheets was excellent. In one instance (Case 6), it was merely fair because only 70% of the entire cultivated epithelial sheet showed mature stratification as determined by fluorescein staining under a phase-contrast microscope and an operating microscope at the end of surgery (Table 1, Figure 1).

• CLINICAL OUTCOMES: All eyes, including the eye transplanted with the sheet whose quality we judged as only fair, demonstrated total re-epithelialization of the corneal surface 2 days after surgery. During the follow-up period, in 10 of 15 eyes the ocular surface grafted with cultivated autologous oral mucosal epithelial sheets remained silent and fairly transparent. However, five eyes, including four with severe SJS, developed small but long-standing epithelial defects; two eyes proceeded to be completely healed by adjacent oral mucosal epithelium, one eye demonstrated conjunctival replacement, and the other two eyes required reoperation. Except for the latter two eyes, all ocular surfaces became stable without any

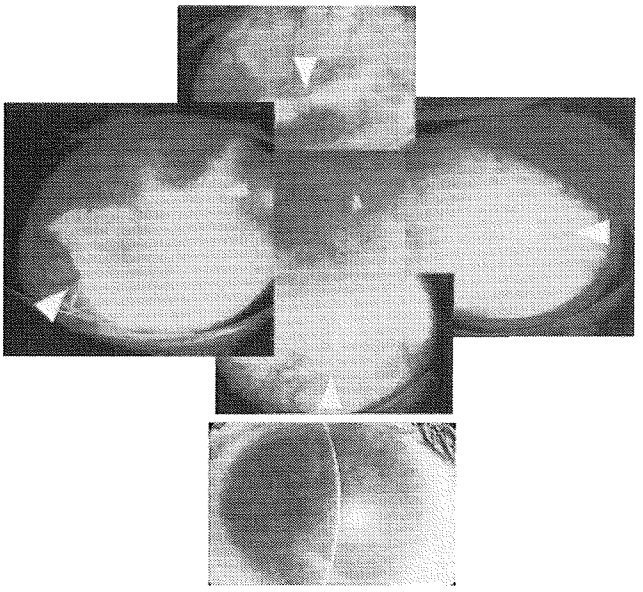

FIGURE 2. The clinical appearance of case 1 at 34 months after cultivated autologous oral mucosal epithelial transplantation. Fluorescein staining confirms the long-term survival of oral mucosal epithelium identified by the different levels of staining density. Arrows indicate the margin of the outgrowth of survived oral mucosal epithelium (Top). Slit-lamp photograph showing the appropriately resurfaced cornea. Note the modest vascularization involving the entire cornea beneath the amniotic membrane sheet and the preexisting corneal stromal opacity (Bottom).

major postoperative complications such as microbial infection or secondary glaucoma (Table 2).

Cultivated corneal epithelial stem cell sheets and ectopically surviving cultivated oral mucosal epithelial sheets are somewhat different in terms of their fluorescein staining patterns at the apical cell surface. In fact, regenerating epithelium that had originated from cultivated oral mucosal epithelium was clearly demarcated from adjacent conjunctival epithelium even as late as 34 months after surgery, the longest follow-up period in this series. This observation strongly suggests the long survival and epithelial supply of presumed oral mucosal epithelial stem cells (Figure 2).

Preoperative best-corrected visual acuity in our series was hand motion (HM) or counting fingers (12 eyes), 20/500 (two eyes), and 20/400 (one eye). Postoperative visual recovery ranged from HM to 20/32; best-corrected visual acuity was improved by more than 2 lines in 10 eyes (67%) at 3 months, and in 10 eyes (67%) at their latest follow-up examination. Three eyes with severe corneal opacity were scheduled for ocular surface reconstruction before penetrating keratoplasty. In cases 9 and 11, we performed a triple procedure with penetrating keratoplasty at 5 and 6 months after the ocular surface reconstruction procedure, respectively; visual acuity achieved in these two eyes was 20/50 and 20/1000. Of the 15 eyes, six were treated with cataract surgery immediately after the removal of ocular surface scarring using either a surgical slit-lamp or a special lighting device, and two eyes were treated with eyelid plastic surgery for entropion attributable to the primary injury (Table 2).

CASE REPORTS

FIGURES 3 AND 4, SHOW REPRESENTATIVE CASES OF CULTIvated autologous oral mucosal epithelial transplantation.

• **CASE 1:** A 33-year-old man in the acute phase of alkali injury graded IIIb with severe corneal stromal opacity in March 2002. AM transplantation was initially performed to cover the total damaged corneal surface, however, persistent corneal epithelial defect and severe inflammation prolonged for more than 1 month. Cultivated autologous oral mucosal epithelial transplantation was performed on June 24, 2002. Postoperatively, the ocular surface showed stabilized epithelialization with peripheral corneal vascularization (Figure 3). Even after 34 months of follow-up, surviving oral mucosal epithelium was distinguishable from conjunctival epithelium. The latest visual acuity was maintained at 10/20.

• **CASE 5:** A 14-year-old girl in the chronic phase of SJS with severe symblepharon over the cornea. The primary SJS occurred at the age of 5. The ocular surface was totally conjunctivalized with severe symblepharon without any surgeries. The ocular surface was reconstructed using cultivated oral mucosal epithelial transplantation, and the postoperative corneal surface was maintained fairly transparent. Best-corrected visual acuity improved from counting fingers to 20/1000 although the damaged corneal stroma was somewhat opaque (Figure 4).

• **CASE 8:** A 61-year-old woman with limbal deficiency of unknown etiology following AM transplantation and conventional allogeneic limbal transplantation. Primary surgery was performed in November 2000, but subsequent failure resulted in total conjunctivalization. After removal of scarred tissue and previously transplanted lenticles, the ocular surface was covered with a cultivated oral mucosal epithelial sheet. Postoperatively, the corneal surface showed complete epithelialization with minimal vascularization; some calcium deposits were observed (Figure 4).

• **CASE 10:** A 65-year-old woman with SJS. The primary SJS occurred at the age of 28. Visual acuity was reduced to CF, because of the conjunctivalization and the progression of cataract. Ocular surface was reconstructed in April 2004 using cultivated oral mucosal epithelial transplantation and cataract surgery. Postoperatively, the ocular surface was stable and transparent (Figure 4). Visual acuity improved to 20/320.